

Giant Acceleration of DNA Diffusion in an Array of Entropic Barriers

Daniel Kim,¹ Clark Bowman,² Jackson T. Del Bonis-O'Donnell,¹ Anastasios Matzavinos,^{2,3} and Derek Stein^{1,*}

¹Department of Physics, Brown University, Providence, Rhode Island 02912, USA

²Division of Applied Mathematics, Brown University, Providence, Rhode Island 02912, USA

³Computational Science and Engineering Laboratory, Department of Mechanical and Process Engineering, CH-8092 ETH Zürich, Switzerland

(Received 22 June 2016; revised manuscript received 8 December 2016; published 27 January 2017)

We investigate with experiments and computer simulations the nonequilibrium dynamics of DNA polymers crossing arrays of entropic barriers in nanofluidic devices in a pressure-driven flow. With increasing driving pressure, the effective diffusivity of DNA rises and then peaks at a value that is many times higher than the equilibrium diffusivity. This is an entropic manifestation of “giant acceleration of diffusion.” The phenomenon is sensitive to the effective energy landscape; thus, it offers a unique probe of entropic barriers in a system driven away from equilibrium.

DOI: 10.1103/PhysRevLett.118.048002

The term “giant acceleration of diffusion” (GAD) refers to a nonequilibrium phenomenon that Brownian particles exhibit in a tilted periodic potential, like the one in Fig. 1(a) [1,2]. The particles’ effective diffusivity peaks at a critical value of the tilt, where it attains a value that can exceed the diffusivity in a uniform potential D_0 by orders of magnitude. GAD has been observed in such varied systems as trapped particles circling corrugated optical vortices [3], colloidal spheres moving across an undulating surface tilted in a gravitational field [4], and the rotating F_1 -ATPase protein motor [5]. It is theoretically predicted that Brownian particles conveyed across *entropic* barriers can exhibit GAD [6–8]; however, this has not been shown experimentally. The entropic case is remarkable because entropic barriers are not fixed; they can change or even vanish as the system is driven away from equilibrium. Here, we report the observation of GAD in the dynamics of DNA polymers driven across arrays of entropic barriers in nanofluidic structures.

A polymer’s configurational entropy varies within a nanofluidic device with an inner topography like the one in Figs. 1(b) and 1(c) [9,10]. A nanofluidic slit with an array of depressions called nanopits gives rise to entropic barriers at the pit edges because more configurations are available to a polymer inside the relatively deep pits than inside the shallow slit, and the entropic penalty for entering the slit is significant when the slit height is smaller than the polymer’s radius of gyration R_g . DNA can fully explore the vertical space inside such devices within milliseconds [11], which is much shorter than its typical dwell time in a pit. Previous theoretical studies highlighted the entropic nature of the barriers polymers encounter in similar geometries [12,13]. Furthermore, in a pressure-driven flow, DNA hops from pit to pit with exponentially distributed dwell times in the pits and a pressure-dependent mobility; this experimentally

observed behavior is consistent with thermally activated transport across entropic barriers [14,15]. Previous studies focused on DNA statistics under nanoconfinement [10,16–22] and DNA mobility in nanotopographies [9,14,21–24] and interpreted the results in terms of the free energy in equilibrium. Here, by contrast, we probe DNA’s diffusivity and its effective energy landscape as it

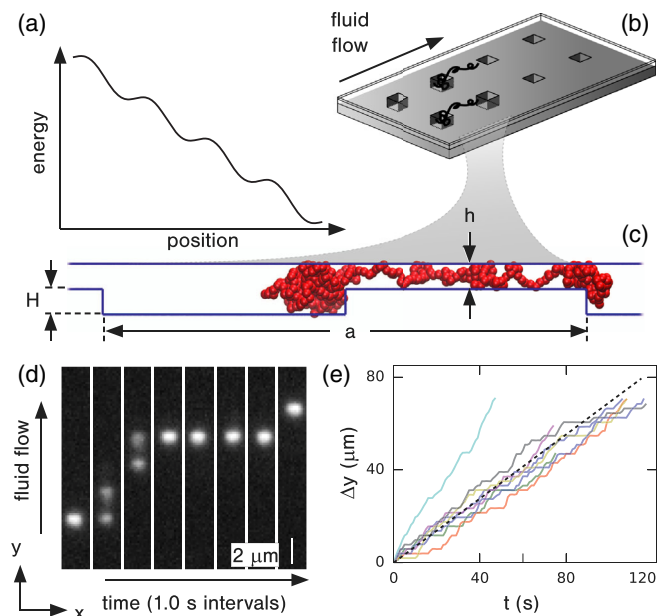


FIG. 1. (a) Sketch of a tilted periodic energy landscape. (b) Illustration of a nanopit array embedded in a nanoslit, with DNA hopping from pit to pit. (c) Side view of the nanofluidic geometry indicating h , H , and a . A simulated polymer hops between pits under an applied drive of $v = 0.05$. (d) Time-sliced fluorescence images of λ DNA climbing a column of high-barrier pits ($h = 75$ nm, $H = 124$ nm) for $\Delta p = 400$ mbar. (e) DNA trajectories from the same experiment. The dashed line indicates $\Delta y = v_p t$ ($v_p = 0.7 \mu\text{m s}^{-1}$).

is driven away from equilibrium. Our experiments and dissipative particle dynamics simulations reveal the piconewton forces at play.

We created arrays of nanopits within nanofluidic slits on fused silica chips, similar to devices described previously [14,25]. The square pits had $1.05 \pm 0.05 \mu\text{m}$ sides and were linearly arrayed with periodicity $a = 2.0 \mu\text{m}$. The depth of a pit relative to the slit controls the height of the entropic barrier. Accordingly, “high” barriers were obtained in one device with slit height $h = 75 \text{ nm}$ and pit depth $H = 124 \text{ nm}$, and a second device with dimensions $h = 88 \text{ nm}$ and $H = 79 \text{ nm}$ had “low” barriers. The terms “low” and “high” are relative comparisons; in both devices, the barriers are higher than the thermal energy $k_B T$, so a pit traps DNA nearly indefinitely without a driving force applied [14]. The slits were 3 mm long and $160 \mu\text{m}$ wide. λ DNA molecules (New England Biolabs), whose contour length is $L = 16.5 \mu\text{m}$ and $R_g = 0.73 \mu\text{m}$ [26], were fluorescently stained with YOYO-1 at a 10:1 base-pair-to-dye ratio and suspended in 20 mM Tris-EDTA buffer titrated to $pH = 8.0$ with HCl, with 3% β mercaptoethanol added. Molecules were driven through the devices by a pressure difference Δp supplied by an air pump. Individual molecules were imaged by epifluorescence microscopy using a $100\times$, 1.49 NA oil-immersion objective (Nikon) and an EMCCD camera (Andor iXon). The excitation light was shuttered with a frequency of 1 Hz and a 50 ms exposure time. Our experimental methods are described in detail in Ref. [14].

Figure 1(d) shows a molecule moving up a column of pits. We tracked the DNA center-of-mass position along the flow direction as a function of time t . Figure 1(e) shows typical trajectories $y(t)$. We tested Δp from 50 to 700 mbar. At each Δp , we recorded 50–80 molecules crossing the pits; more than 2000 total pit-to-pit hops were typically observed in order to obtain good estimates of the mean velocity and the diffusion coefficient. 12–20 molecules were also recorded crossing pit-free regions of the slit, where the flow velocity is proportional to Δp . The mean DNA velocity in the slit is v_s ; we used v_s to quantify the driving force rather than Δp because manometer readings of the latter were less consistent.

To quantify the DNA diffusivity, we first evaluated the drift-subtracted mean square displacement (MSD) for each ensemble of trajectories,

$$\text{MSD} = \langle [\Delta y(\tau) - v_p \tau]^2 \rangle, \quad (1)$$

where $\Delta y(\tau)$ is a molecule’s y displacement in the time interval τ , $\langle \dots \rangle$ indicates an ensemble average, and v_p is the mean DNA velocity across the pits. (See Supplemental Material [27], which includes Refs. [28,29], for details and comparisons with alternative analysis methods.) The effective diffusivity D is related to MSD by

$$D \equiv \lim_{\tau \rightarrow \infty} \text{MSD}/2\tau. \quad (2)$$

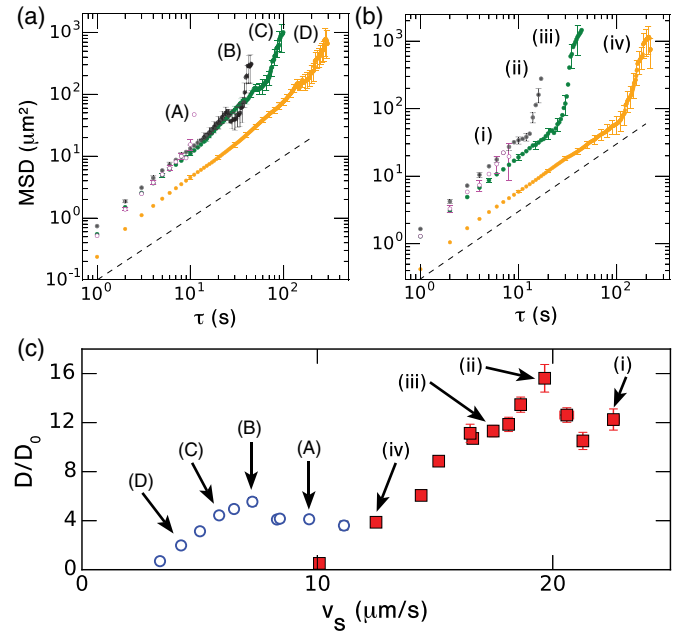


FIG. 2. Dependence of MSD on τ in (a) the device with low barriers for $\Delta p = 250$ (A), 140 (B), 90 (C), and 60 mbar (D). And in (b) the device with high barriers for $\Delta p = 750$ (i), 650 (ii), 555 (iii), and 400 mbar (iv). The corresponding D/D_0 and v_s are indicated in (c). The dashed line has a slope of 1. (c) Dependence of D/D_0 on v_s for low (blue dots) and high (red squares) barriers with $\tau = 2 \text{ s}$. Error bars are the standard error from a bootstrap analysis of 200 resamplings of the full data set.

Figures 2(a) and 2(b) show the growth of MSD with τ in devices with low and high barriers, respectively, at four Δp each. On the log-log plot, MSD increased linearly with τ with a slope near 1. For each Δp , there was an upper experimental limit to τ , beyond which MSD rose sharply. That limit corresponded to the time it took the fastest molecules to exit the camera’s field of view, which decreased as Δp increased. To compare measurements on an equal basis, we evaluated D using Eq. (2) with $\tau = 2 \text{ s}$. We verified that velocity autocorrelations are negligible for $\tau = 2 \text{ s}$ and that D is relatively insensitive to τ (see Supplemental Material [27]). The self-diffusion of DNA in a slit with $\Delta p = 0$ could be observed for long times, so we obtained D_0 from the slope of MSD versus τ (see Supplemental Material [27]); we found $D_0 = 0.084 \mu\text{m}^2 \text{ s}^{-1}$ in the $h = 88 \text{ nm}$ slit and $D_0 = 0.067 \mu\text{m}^2 \text{ s}^{-1}$ in the $h = 75 \text{ nm}$ slit.

Figure 2(c) shows the dependence of D/D_0 on v_s . In both devices, D/D_0 increased with v_s from zero to a peak, after which D/D_0 decreased. The peak occurred at $v_s = 7.2 \mu\text{m s}^{-1}$ in the device with low barriers and at $v_s = 19.7 \mu\text{m s}^{-1}$ in the device with high barriers. The height of the D/D_0 peak also depended on the nanotopography; it reached ≈ 5.5 in the device with low barriers and ≈ 15.5 in the one with high barriers.

A nonmonotonic dependence of D on driving force (i.e., tilt) is a hallmark of GAD [2]. The theory is based on the

Langevin equation for an overdamped Brownian particle in a periodic potential, $G(y) = G(y + a)$, with a constant tilt force F ,

$$\zeta \frac{dy}{dt} = -\frac{dG(y)}{dy} + F + f(t), \quad (3)$$

where ζ is the drag coefficient and $f(t)$ is the random force from thermal fluctuations, defined by the moments $\langle f(t) \rangle = 0$ and $\langle f(t)f(t') \rangle = 2\zeta k_B T \delta(t-t')$, where $\delta(t-t')$ is Dirac's delta function centered at t' [30]. Reimann *et al.* showed that the dynamics are governed by the form of $G(y)$ near the critical point, which is the dynamical bottleneck [2]. They expanded $G(y)$ about the critical point, chosen to be $y_c = 0$, to obtain the small y behavior

$$G(y) - yF = -\mu y|y|^{q-1} - y\epsilon, \quad (4)$$

where $q > 0$, $\mu > 0$ characterizes the gradient of the potential force near y_c , and $\epsilon \equiv F - F_c$. Equation (4) leads to the following expression for D/D_0 [2]:

$$\frac{D}{D_0} = \left(\frac{a^q \mu}{k_B T} \right)^{2/q} \frac{\int_{-\infty}^{\infty} dy K^2(y, \gamma) K(-y, \gamma)}{[\int_{-\infty}^{\infty} dy K(y, \gamma)]^3}, \quad (5)$$

where $K(y, \gamma) \equiv \int_0^{\infty} dy' e^{-\gamma|y|^{q-1} + (y-y')|y-y'|^{q-1} - \gamma y'}$ and $\gamma \equiv \epsilon/[\mu^{1/q}(k_B T)^{1-1/q}]$. In the generic case, $G(y)$ is an analytic function and $q = 3$. D is a peaked function of F , with the peak occurring at $F \approx F_c$.

The peak corresponds to particles alternating between trapped and freely running states. When F is very low, particles become trapped between energy barriers and D is suppressed. Increasing F lowers the forward energy barrier and facilitates downhill motion. F_c is where the barrier vanishes. Beyond that, particles can run freely and D approaches D_0 .

The DNA dynamics in nanopit arrays can be mapped onto GAD theory by casting the effective free-energy landscape for DNA, $\Psi(y)$, in the role of $G(y) - yF$. The entropic barriers give a periodic contribution $S(y)$ to $\Psi(y)$. The viscous driving force is nonconservative, but we can define an effective potential $V(y)$ for it through the work required to translate a molecule adiabatically against the viscous force [14]. $V(y)$ must be proportional to v_s . It can be written as the difference of two terms, $V(y) = U(y)v_s - y\zeta^*v_s$, where $U(y)$ is a periodic function related to the periodically varying flow speed inside the nanopit array and ζ^* is an effective drag that quantifies the net force downstream. Combining the contributions, $\Psi(y)$ becomes

$$\Psi(y) = S(y) + U(y)v_s - y\zeta^*v_s. \quad (6)$$

Equation (6) describes the competition between entropy and enthalpy. Inertial effects are absent because the Reynolds number in nanofluidic systems is extremely low. With these definitions, DNA obeys Eq. (3), with $G(y) = S(y) + U(y)v_s$ and $F = \zeta^*v_s$. Furthermore,

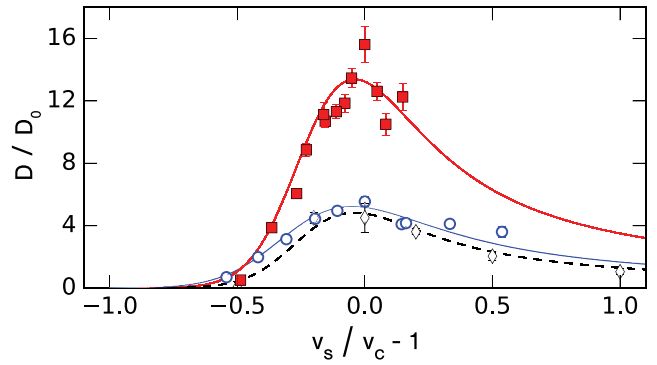


FIG. 3. Dependence of D/D_0 on $v_s/v_c - 1$ in devices with high (red squares) and low (blue dots) barriers, and for simulation data (diamonds). The lines are fits of Eq. (5) to the corresponding data, with fit parameters μ and F_c .

Eq. (5) gives the effective diffusivity of DNA with $\mu = -\frac{1}{6}[S'''(0) + U'''(0)v_s]$ and $\epsilon = [\zeta^* - U'(0)](v_s - v_c)$ (primes indicate derivatives; see Supplemental Material [27] for the derivation, which includes Refs. [28,31]).

We fit Eq. (5) to D/D_0 using μ and F_c as fitting parameters and assuming $q = 3$. The device with high barriers obtained $\mu = 1.00k_B T a^{-3}$ and $F_c = 0.18$ pN. The device with low barriers obtained $\mu = 0.21k_B T a^{-3}$ and $F_c = 0.08$ pN. Figure 3 shows D/D_0 from both devices as a function of the rescaled slit velocity $v_s/v_c - 1$, where v_c is the mean slit speed at the peak. Also shown is Eq. (5) with the fit values of μ and F_c . The shape of Eq. (5) agrees very well with the data.

To investigate the nonequilibrium forces that DNA experiences and how well those are described by an effective potential landscape, we performed computer simulations that approximate the experiments. The system was modeled using dissipative particle dynamics, a type of coarse-grained molecular dynamics commonly used for applications in nanofluidics [32–35]. A section of the device comprising three consecutive pits in the slit, partly shown in Fig. 1(c), was filled with water particles using the standard parameters established by Groot and Warren [36]. We modeled λ DNA as a bead-spring polymer with 660 beads and matched its proportions to the device geometry. A harmonic bending energy was imposed to give the polymer a comparable R_g to that of the DNA in the experiments. The dimensions of the pits and slit corresponded to a device having $1.0 \mu\text{m}$ wide pits, periodicity $a = 2.0 \mu\text{m}$, and $H = h = 100$ nm. Partial-slip boundary conditions were imposed on the top and bottom boundaries according to the method of Pivkin and Karniadakis [37]. Finally, a uniform, time-varying force was applied to fluid in the upper half of the device (the slit) to create the flow. The force was adjusted to achieve a target mean fluid velocity v . Periodic boundaries in the flow direction ensured that fluid did not escape the system. The system was evolved in time using a velocity Verlet scheme [32].

We simulated a range of v . We sampled the polymer's center-of-mass position at regular intervals, computed MSD, used it to determine D , and then fit the data to Eq. (5) as before. The sampling rate, corresponding to τ in the previous analysis, was chosen so that the average number of pit-to-pit hops per τ was comparable to the experimental data. Figure 3 shows D/D_0 and the fit to Eq. (5) from the simulations. The simulation data closely matched the behavior in the device with low barriers, whose proportions it approximated.

Our computer simulations permitted deeper analysis of the underlying forces, which could not be measured experimentally. We tracked the total force on the simulated polymer, $F_{\text{total}}(y, t)$, and mapped it to our analytical model:

$$F_{\text{total}}(y, t) \approx -\zeta \frac{dy}{dt} - \frac{d\Psi(y)}{dy} + f(t). \quad (7)$$

The first term on the right-hand side is the viscous drag force, the second term is the potential force, and the third term is the random thermal force. The effective force from the energy landscape can be obtained by ensemble averaging the simulation data:

$$-\frac{d\Psi(y)}{dy} \approx \left\langle \zeta \frac{dy}{dt} + F_{\text{total}}(y, t) \right\rangle_i. \quad (8)$$

Simulations were run below ($v = 0.04$ simulation units), near ($v = 0.05$), and above ($v = 0.06$) the velocity of peak diffusivity, with the goal of observing changes in the effective force landscape as the critical v is passed. For each simulation, the velocity autocorrelation function $\langle v(t)v(t+\tau) \rangle$ was calculated. For small τ , this function decays exponentially with $(\zeta/m)\tau$, where m is the particle mass. By matching this exponent with the simulation data, effective values of ζ were calculated for each simulation. We found $\zeta = 147.7, 140.4,$ and 138.5 for $v = 0.04, 0.05,$ and 0.06 , respectively (see Supplemental Material for details [27]). For each simulation, we binned data by the center-of-mass y position using adaptive bins, which equalized the number of data in each bin. Using the calculated values of ζ and the mean values of $F_{\text{total}}, dy/dt,$ and position within each bin, we generated approximate potential force landscapes according to Eq. (8).

Figure 4(a) shows a simulated polymer trapped near the critical point and Fig. 4(b) plots the potential force landscapes. For the subcritical $v = 0.04$, a portion of the force landscape is negative, i.e., opposing the direction of motion. As v increases, this minimum force shifts upward, crossing through zero. In particular, the potential force minimum was closest to zero as the diffusivity reached its peak at $v = 0.05$. The minima of all three landscapes occurred around $y \approx 55$, where the DNA molecule would become trapped—pushed up against the forward wall of the pit—before escaping.

In the theory of Reimann *et al.*, the dynamical bottleneck also governs the drift velocity [2]:

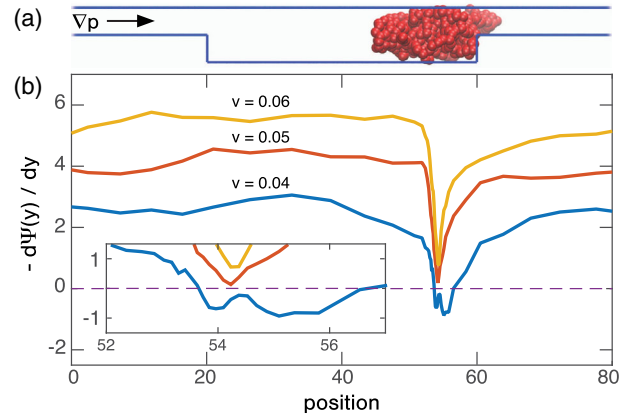


FIG. 4. (a) Side view of a simulated polymer inside a nanofluidic device, near the critical point, with $v = 0.05$. (b) Effective force landscapes $-d\Psi(y)/dy$ for $v = 0.04, 0.05,$ and 0.06 (labeled curves), computed from Eq. (8). The position axis is aligned with the nanofluidic geometry in (a). The inset shows an expanded view of the force landscape around the critical point. The dashed line indicates zero force.

$$v_p = \frac{1 - e^{-aF/k_B T}}{\int_{-\infty}^{\infty} dy K(y, \gamma)}. \quad (9)$$

As a final test, we compare in Fig. 5 v_p from the experiments and simulations with Eq. (9), using the previously fit values of μ and F_c . The data are rescaled by $v_0 = v_s/(1 + H/2h)$, the approximate limiting velocity, and plotted against F/F_c . Figure 5 shows good agreement between the model and the data.

Entropic barriers develop at the nanopit edges and give rise to GAD because the polymer can rapidly sample the changing height inside the device (see the video in Supplemental Material [27]). The situation is akin to Brownian particles in an undulating geometry, which are predicted to exhibit GAD *if* the equilibration in the transverse dimension is relatively quick [6]. We note that Eq. (9) seems to become less accurate at high v_s in Fig. 5.

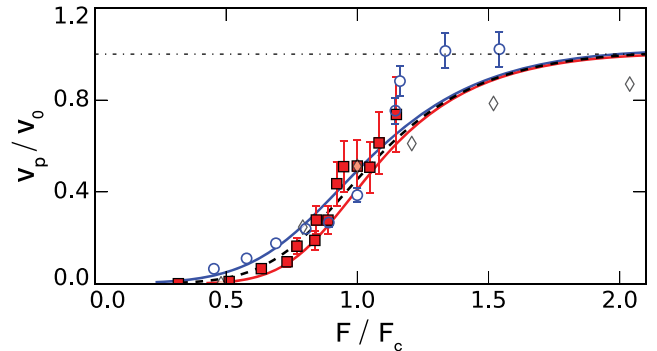


FIG. 5. Dependence of v_p/v_0 on F/F_c in devices with high (red squares) and low (blue dots) barriers, and simulation data (black diamonds). The corresponding lines plot Eq. (9) using the fit values of μ and F_c . The dot-dashed line shows $v_p/v_0 = 1$.

The shape of the force landscapes in Fig. 4 also changes noticeably as v increases, with a sharper barrier developing near the critical point. These effects hint at a changing entropic barrier as the polymer is driven further from equilibrium.

In conclusion, we have demonstrated giant acceleration of diffusion, a nonequilibrium dynamical phenomenon, in a system with *entropic* barriers. GAD remarkably enables measurements of subpiconewton forces acting on a single molecule by simply observing its motion. GAD also creates an opportunity to study entropic barriers by revealing the shape of the free-energy landscape near the critical point. Future work should seek to understand how entropic barriers change with the driving force and investigate the possible emergence of nonideal behavior. Nanofluidics is a convenient arena for studying GAD and other nonequilibrium phenomena. Such work could lead to useful new ways of controlling molecules.

The authors thank J. Lee for assistance with image analysis. D. K., J. T. D., and D. S. acknowledge support from NSF under Grant No. 1409577. A. M. and C. B. acknowledge support from NSF under Grant No. 1552903 and No. 1521266. A. M. thanks the Computational Science and Engineering Laboratory at ETH Zürich for their warm hospitality. Part of this research was conducted using the computational resources and services at the Center for Computation and Visualization, Brown University.

*derek_stein@brown.edu

- [1] G. Costantini and F. Marchesoni, *Europhys. Lett.* **48**, 491 (1999).
- [2] P. Reimann, C. Van den Broeck, H. Linke, P. Hänggi, J. M. Rubi, and A. Pérez-Madrid, *Phys. Rev. Lett.* **87**, 010602 (2001).
- [3] S. H. Lee and D. G. Grier, *Phys. Rev. Lett.* **96**, 190601 (2006).
- [4] X. G. Ma, P. Y. Lai, B. J. Ackerson, and P. Tong, *Phys. Rev. E* **91**, 042306 (2015).
- [5] R. Hayashi, K. Sasaki, S. Nakamura, S. Kudo, Y. Inoue, H. Noji, and K. Hayashi, *Phys. Rev. Lett.* **114**, 248101 (2015).
- [6] D. Reguera, G. Schmid, P. S. Burada, J. M. Rubí, P. Reimann, and P. Hänggi, *Phys. Rev. Lett.* **96**, 130603 (2006).
- [7] P. S. Burada, G. Schmid, D. Reguera, M. H. Vainstein, J. M. Rubi, and P. Hänggi, *Phys. Rev. Lett.* **101**, 130602 (2008).
- [8] J. Sancho and A. Lacasta, *Eur. Phys. J. Spec. Top.* **187**, 49 (2010).
- [9] J. Han and H. G. Craighead, *Science* **288**, 1026 (2000).
- [10] W. Reisner, N. B. Larsen, H. Flyvbjerg, J. O. Tegenfeldt, and A. Kristensen, *Proc. Natl. Acad. Sci. U.S.A.* **106**, 79 (2009).
- [11] M. Doi and S. F. Edwards, in *The Theory of Polymer Dynamics*, International Series of Monographs on Physics (Clarendon Press, Oxford, 1986).
- [12] S. T. T. Ollila, C. Denniston, M. Karttunen, and T. Ala-Nissila, *Phys. Rev. Lett.* **112**, 118301 (2014).
- [13] G. I. Nixon and G. W. Slater, *Phys. Rev. E* **53**, 4969 (1996).
- [14] J. T. D. Bonis-O'Donnell, W. Reisner, and D. Stein, *New J. Phys.* **11**, 075032 (2009).
- [15] C. L. Vestergaard, M. B. Mikkelsen, W. Reisner, A. Kristensen, and H. Flyvbjerg, *Nat. Commun.* **7**, 10227 (2016).
- [16] T. Odijk, *Phys. Rev. E* **77**, 060901 (2008).
- [17] L. Dai, J. J. Jones, J. R. C. van der Maarel, and P. S. Doyle, *Soft Matter* **8**, 2972 (2012).
- [18] J. Tang, S. L. Levy, D. W. Trahan, J. J. Jones, H. G. Craighead, and P. S. Doyle, *Macromolecules* **43**, 7368 (2010).
- [19] J. O. Tegenfeldt, C. Prinz, H. Cao, S. Chou, W. W. Reisner, R. Riehn, Y. M. Wang, E. C. Cox, J. C. Sturm, P. Silberzan, and R. H. Austin, *Proc. Natl. Acad. Sci. U.S.A.* **101**, 10979 (2004).
- [20] E. A. Strychalski, S. L. Levy, and H. G. Craighead, *Macromolecules* **41**, 7716 (2008).
- [21] S. L. Levy and H. G. Craighead, *Chem. Soc. Rev.* **39**, 1133 (2010).
- [22] L. Wu and S. Levy, *Biomicrofluidics* **8**, 044103 (2014).
- [23] J. Han, S. Turner, and H. Craighead, *Phys. Rev. Lett.* **83**, 1688 (1999); **86**, 1394 (2001).
- [24] P. G. de Gennes, in *Polymers in Confined Environments*, edited by S. Granick, K. Binder, P. G. de Gennes, E. P. Giannelis, G. S. Grest, H. Hervet, R. Krishnamoorti, L. Leger, E. Manias, E. Raphael, and S. Q. Wang (Springer, Berlin, 1999) pp. 91–105.
- [25] E. Shelton, Z. Jiang, S. Wang, and D. Stein, *Appl. Phys. Lett.* **99**, 263112 (2011).
- [26] D. Smith, T. Perkins, and S. Chu, *Macromolecules* **29**, 1372 (1996).
- [27] See Supplemental Material at <http://link.aps.org/supplemental/10.1103/PhysRevLett.118.048002> for details of the calculations of v_p , D , and D_0 from DNA trajectories, comparisons with alternative approaches to computing MSD and v_p , the dependence of D/D_0 on the choice of τ , the theoretical mapping of the dynamics of DNA in nanopit arrays to GAD theory, including the case of spatially varying drag coefficient, calculations of the effective drag coefficient of simulated polymers, and a video of simulated polymers traversing the nanopit array both below and above the diffusivity peak.
- [28] A. Balducci, P. Mao, J. Han, and P. S. Doyle, *Macromolecules* **39**, 6273 (2006).
- [29] H. Qian, M. Sheetz, and E. Elson, *Biophys. J.* **60**, 910 (1991).
- [30] R. Zwanzig, *Nonequilibrium Statistical Mechanics* (Oxford University Press, New York, 2001).
- [31] M. Chipot, *Elliptic Equations: An Introductory Course* (Birkhäuser, Basel, 2009).
- [32] G. E. Karniadakis, A. Beskok, and N. Aluru, *Microflows and Nanoflows: Fundamentals and Simulation* (Springer Science & Business Media, Basel, 2006), Vol. 29.
- [33] E. Moeendarbary, T. Y. Ng, and M. Zangeneh, *Int. J. Appl. Mech.* **02**, 161 (2010).
- [34] P. Español, *Phys. Rev. E* **52**, 1734 (1995).
- [35] P. Español and P. Warren, *Europhys. Lett.* **30**, 191 (1995).
- [36] R. D. Groot and P. B. Warren, *J. Chem. Phys.* **107**, 4423 (1997).
- [37] I. V. Pivkin and G. E. Karniadakis, *J. Comput. Phys.* **207**, 114 (2005).